TSINGHUA SCIENCE AND TECHNOLOGY
ISSN 1007-0214 18/20 pp883–896
DOI: 10.26599/TST.2023.9010047
Volume 29, Number 3, June 2024

An Electrical Impedance Imaging System Towards Edge Intelligence for Non-Destructive Testing of Concrete

Abolfazl Roshanpanah, Mahdi Abbasi*, Hani Attar, Ayman Amer, Mohammad R. Khosravi, and Ahmed A. Solyman

Abstract: In the construction industry, to prevent accidents, non-destructive tests are necessary and cost-effective. Electrical impedance tomography is a new technology in non-invasive imaging in which the image of the inner part of conductive bodies is reconstructed by the arrays of external electrodes that are connected on the periphery of the object. The equipment is cheap, fast, and edge compatible. In this imaging method, the image of electrical conductivity distribution (or its opposite; electrical impedance) of the internal parts of the target object is reconstructed. The image reconstruction process is performed by injecting a precise electric current to the peripheral boundaries of the object, measuring the peripheral voltages induced from it and processing the collected data. In an electrical impedance tomography system, the voltages measured in the peripheral boundaries have a non-linear equation with the electrical conductivity distribution. This paper presents a cheap Electrical Impedance Tomography (EIT) instrument for detecting impurities in the concrete. A voltage-controlled current source, a micro-controller, a set of multiplexers, a set of electrodes, and a personal computer constitute the structure of the system. The conducted tests on concrete with impurities show that the designed EIT system can reveal impurities with a good accuracy in a reasonable time.

Key words: non-destructive testing system; concrete; electrical impedance tomography

1 Introduction

Imaging methods of the internal tissues of the target object are called tomography[1]. These methods are frequently used in power-efficient embedded devices in edge layer of Internet of Medical Things (IoMT)[2, 3]. Among these methods are X-ray tomography[4, 5], positron tomography[6], Magnetic Resonance Imaging (MRI)[7], and ultrasound tomography[8, 9]. In each of these methods, a specific feature of the target object is depicted[10, 11]. It is worth to mention that many of recent imaging technologies are deployed in the form of web APIs or mobile applications[12]. The big data,

• Abolfazl Roshanpanah is with Department of Electrical Engineering, Islamic Azad University, Science and Research Brance, Tehran 1477893855, Iran. E-mail: a.roshanpanah@srbiau.ac.ir.
• Mahdi Abbasi is with Department of Computer Engineering, Bu-Ali Sina University, Hamedan 6517838695, Iran. E-mail: abbasi@basu.ac.ir.
• Hani Attar and Ayman Amer are with Department of Energy Engineering, Zarqa University, Zarqa 13110, Jordan. E-mail: Hattar@zu.edu.jo; Aamer@zu.edu.jo.
• Mohammad R. Khosravi is with Department of Computer Engineering, Persian Gulf University, Bushehr 7516913817, Iran. E-mail: mohammadkhosravi@acm.org.
• Ahmed A. Solyman is with Department of Electrical and Electronics Engineering, Faculty of Engineering and Architecture, Nişantaşı University, Istanbul 34398, Turkey. E-mail: ahmed.solyman@nisantasi.edu.tr.
* To whom correspondence should be addressed.
Manuscript received: 2023-04-01; revised: 2023-05-18; accepted: 2023-05-23

generated by such medical applications, pose challenges in image processing[13], power-efficient, and intelligent data mining and communication methods[14–16].

In Electrical Impedance Tomography (EIT), the quantity depicted is the impedance or electrical conductivity of the internal tissues of the target object[8, 17].

Figure 1 shows the general structure of an EIT system. Electrical energy is sent to the human body with weak currents, and the voltage induced in the electrodes is measured. The means of sending and receiving signals are electrodes. By using the EIT imaging method, it is possible to image the internal part of objects, such as concrete structures or the inside of the human body. With the advent remote structural health monitoring and non-destructive testing impedance, imaging is considered as an efficient method[18, 19] with enough security in complex environment[19]. The output of the EIT system is an image of the electrical conductivity distribution inside the target object. Various conventions have been proposed for current injection and voltage measurement on the electrodes. These contracts are divided into two general categories: double reading and multiple reading[17, 20].

Systems based on double reading direct the current generated from a current source to the terminals of two driving electrodes, and measure the voltage on the other electrodes. In such systems, the voltage measured on the driving electrodes is not used due to the presence of noise[8].

After a voltage frame is collected, the current is injected through two other electrodes, and thus the measurement is done with all electrodes[8, 17]. Such systems are also called applied potential tomography systems[21]. Among the most important APT systems are Sheffield Mark 1 from Sheffield University[22] and KHU Mark 1[23] from Kung Hi University.

Systems based on multiple readings are more expensive and complex, having more than one source of current injection, thereby stimulating more than one pair of electrodes for current injection[1, 17].

In both types of electrode stimulation and voltage measurement, if the number of electrodes is equal, the total number of possible measurements will be equal. By deducting the noisy measurements performed on the current injecting electrodes, this number reaches $L(L-1)$, where L is the number of electrodes, and considering the principle of measurement opposition, this number is reduced to $L(L-3)/2$[24]. To measure cross-sectional impedance in a system based on double reading, electrodes are placed on the same surface around the object and inject current and measure voltage[8, 17, 25].

This paper presents a low-cost and efficient design for a 16-electrode impedance imaging system and an experimental phantom. The system is intended to be used in non-destructive testing of concrete via measuring any inhomogeneous impedance pattern caused by cracks in the concrete or cement mixtures. The experimental results confirm the accuracy and efficiency of the instrumented prototype.

This article is presented as follows. The order of

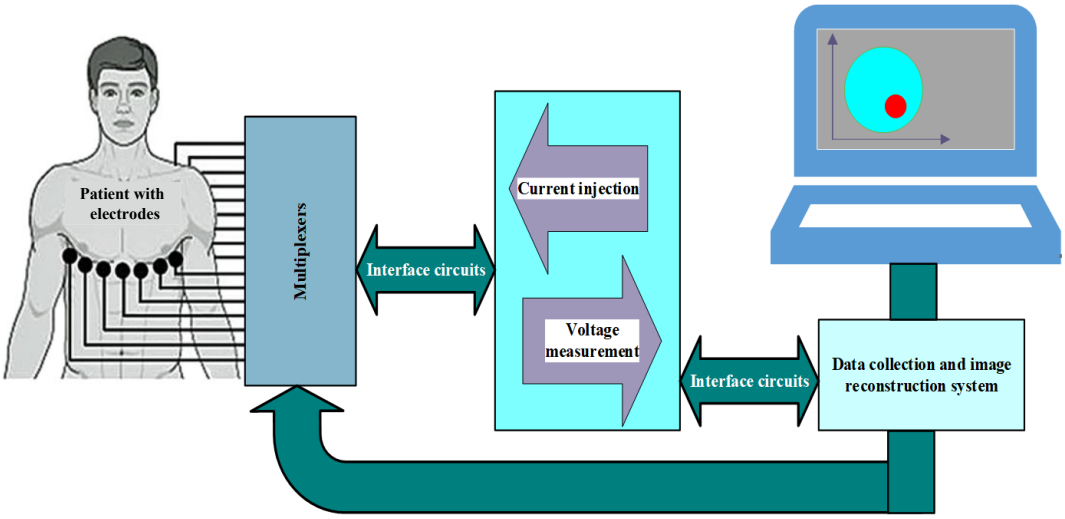

Fig. 1 Structure of an electrical impedance imaging system[8].

presenting the sections is based on the order of the work done during this research. Section 2 is devoted to the investigation of the mathematical foundations of the electric impedance tomography problem. In this section, the governing equation of the problem is determined. After introducing the electrode models and boundary conditions of the problem, the forward and inverse problems of impedance tomography are explained. In Section 3, with the electrode patterns introduced, the complete electrode model is reviewed. In Section 4, the electrical properties of concrete and electrical conductivity in materials containing cement are investigated, and the electrical equivalent circuit of cracks in concrete structures and its governing equations are introduced. In Section 5, after the EIT system hardware is introduced, the process of data collection and image reconstruction is described. Section 6 includes five different tests to evaluate the correctness of the system's performance. The experimental tests are based on the current and voltage measured on specific impedance models as boundary data. Section 7 summarizes and presents the important results of the research.

2 Mathematical Foundations of EIT Problem

2.1 Mathematical model of an EIT problem

Unlike other tomography methods, electrical impedance imaging is non-local. This means that the change of electrical conductivity in a part of the body affects the measured voltage in all electrodes in a non-linear way[3, 5].

According to Hadamard's definition, the mathematical model of a well-posed physical problem has the following conditions[26–28]:

(1) For each data, the problem has one answer.

(2) The answer is unique.

(3) The answer depends continuously on the data of the problem.

If the above conditions are violated in the mathematical model of a problem, that problem is called an ill-posed problem. The problem of reconstructing the image of the impedance inside the object based on the voltage and current measured by the electrodes around it, according to Hadamard's third condition, is an ill-posed problem.

Reconstructing the electrical impedance image is a non-linear problem. This means if the voltages obtained on similar electrodes around two bodies with two different values of electric conductance, as a result of injecting a specific current pattern, are added together separately, they are not equal to the voltages resulting from injecting current on an object whose electrical conductivity is equal to the sum of the electrical conductivity of the two mentioned objects[9].

Electromagnetism problems are expressed based on Maxwell's equations. Maxwell's equations about electric field E and magnetic field H about a body Ω are as follows:

$$\nabla \times E = -\mathrm{i}\omega B \tag{1}$$

$$\nabla \times H = J + \mathrm{i}\omega D \tag{2}$$

where ω is the angular frequency in Hz, B is the magnetic flux density, J is the electric current density in terms of $\frac{A}{m^2}$, and D is the electric displacement in terms of $\frac{C}{m^2}$[29, 30]:

According to Stokes law, at any point of two-dimensional space with vector coordinates r, the relationship between electric field and electric potential u is expressed as follows:

$$-\nabla u(r) = E(r) \tag{3}$$

On the other hand, electric displacement and electric current density can be expressed based on the electric field with the following equations:

$$D = \epsilon E \tag{4}$$

$$J = \sigma E \tag{5}$$

where ϵ is the electrical permeability coefficient of the object and σ is the electrical conductivity coefficient of the object.

Considering Eqs. (4) and (5), Eq. (2) is rewritten in the following form:

$$\nabla \times H = (\sigma + \mathrm{i}\epsilon\omega) E \tag{6}$$

In this regard, the complex parameter $\sigma + \mathrm{i}\epsilon\omega$ is the electrical conductivity coefficient of the object. Since for any vector field H,

$$\nabla (\nabla \times H) = 0 \tag{7}$$

Equations (3) and (6) are used to get the following equation:

$$\nabla ((\sigma + \mathrm{i}\epsilon\omega) \nabla u(r)) = 0 \tag{8}$$

which is a Laplace equation. Considering that the frequencies used in EIT are low, the quasi-static

approximation can be used, meaning that the capacitive diffusion and inductive effects are ignored, and Eq. (8) can be presented in the following form:

$$\nabla(\sigma\nabla u(r)) = 0 \tag{9}$$

This equation determines the electric potential $u(r)$ at each point $r \in \Omega$. Practically, a current with a specific amplitude and phase is applied to the electrodes around the object. The applied current creates a current density outward in the direction perpendicular to the surface of the boundary of the object, whose distribution is shown by g. Therefore, the boundary conditions of the problem are as

$$\sigma \left.\frac{\partial u}{\partial n}\right|_{\partial\Omega} = g, \quad u|_{\partial\Omega} = f \tag{10}$$

where n denotes the outward unit normal. Mathematically, the EIT problem is expressed in the form of Laplace's Eq. (9) with Newman's boundary conditions in Eq. (10). Due to the use of the finite element approach in solving the forward problem, the definition of the weak response is presented as follows.

Definition 1 We consider u as the potential function, which is resulted by solving Eq. (9). For each test function, v denotes any test voltage induced on the surface of the conductive surface ω, and $v \in \mathbf{C}_0^\infty$ is satisfied in the following equation:

$$\int_\Omega \sigma\nabla u\nabla v \, \mathrm{d}r = 0 \tag{11}$$

In this definition, H^1 is the space of continuous and integrable functions, and $\mathbf{C}_0^\infty(\Omega)$ is the space of continuous functions with limited domain in Ω[29].

2.2 Electrode models

In EIT, the signal-to-noise ratio is proportional to the square of the ratio of the peripheral area covered by the electrodes[25, 30]. The presence of highly conductive electrodes on the surface of the object, creates effective proofs for the movement of current on the surface of the object, and reduces the current density inside the object. Therefore, the presence of electrodes in the mathematical equation must be accurately modeled. The use of more accurate models of electrodes makes it possible to accurately express the boundary conditions of the problem.

Several models for electrodes have been presented[25, 30, 31]. Some of the most important models presented are the continuous model, the gap model, the parallel resistance model, and the Complete Electrode Model (CEM). For the first time, these models were examined and presented by Cheng et al.[31] In these models, the electrical impedance measurement system includes the object Ω to be measured, number of surrounding electrodes denoted by L, and the current injection and voltage measurement tools.

The complete electrode model involves the contact impedance of the electrode with the object in the equations. If the current injecting electrode is used to measure the voltage, it is necessary to consider the contact impedance of the electrode. In this model, the potential u meets the following conditions:

- Condition of the current injecting electrodes: In this model, the current intensity in the current injecting electrodes is assumed to be constant,

$$I = \int_{E_j} (\sigma\nabla u) n \, \mathrm{d}s = -\int_{E_{j+1}} (\sigma\nabla u) n \, \mathrm{d}s \tag{12}$$

where I denotes the current intensity in the current injecting electrodes.

- Condition of surface without electrodes: the intensity of the current in the surface without electrodes is zero,

$$\sigma\frac{\partial u}{\partial n} \text{ on } \partial\Omega \setminus \bigcup_{k=1}^{L} E_k \tag{13}$$

where E_k denotes the surface under the k-th electrode.

- Voltage measurement electrodes: the effect of contact impedance with the object is considered Z_k in the measured potential,

$$u + z_k \left(\sigma\frac{\partial u}{\partial n}\right)\Big|_{E_k} = U_k, \quad k = 1, 2, \ldots, L \tag{14}$$

where U_k is the voltage measured on the electrode number k. Considering one of the electrodes as the reference electrode, the following condition can be taken as a complement to the third boundary condition,

$$\sum_{k=1}^{L} U_k = 0 \tag{15}$$

It should be noted that this condition is necessary for the uniqueness of the answer of Laplace's equation.

- All electrodes: the potential u in each electrode (providing high electrical conductivity) is constant,

$$\int_{E_k} \sigma\frac{\partial u}{\partial n}\mathrm{d}s = 0, \quad k \in \{1, 2, \ldots, L\} \setminus \{j, j+1\} \tag{16}$$

In an electrical impedance measurement system with a reference electrode, the measured voltages are as follows:

$$\begin{aligned} V^{j,1} &:= U_1^j - U_2^j, \\ V^{j,2} &:= U_2^j - U_3^j, \\ &\vdots \\ V^{j,L} &:= U_L^j - U_1^j \end{aligned} \tag{17}$$

The index j in the above expressions indicates the current injection pattern number. In fact, electrodes j and $j+1$ are used for current injection and the voltage difference defined in Eq. (17) is measured simultaneously on the electrodes $1, 2, \ldots, L$. In an electrical impedance tomography system, some current patterns are injected into the body through a pair of adjacent electrodes $I_1, I_2, \ldots, I_L$, and a series of voltages are measured, which can be displayed in the discrete form below:

$$F(\sigma) = \begin{bmatrix} V^{1,1}, \cdots, V^{1,L} \\ \ddots \\ V^{L,1}, \cdots, V^{L,L} \end{bmatrix} \tag{18}$$

The above relationship states that voltage values are influenced by contact impedance. According to the principle of duality $V^{j,k} = V^{k,j}$, the maximum number of independent data F is equal to $L(L-1)/2$[8, 32].

2.3 Forward and inverse problems

According to the definition of the complete electrode model, it can be seen that in this model there are two different types of boundary data that are connected through u and σ. Therefore, the following definition can be given.

Definition 2 A binary (f, g) is called a continuous boundary data, and (U_l, I_l), $l = 1, 2, \ldots, L$ is also called a discrete boundary data. A part of a pair is compatible with the other part if the values of u and σ are found, such that the conditions of Eqs. (11) and (12) and also the corresponding conditions of Eqs. (14) to (18) are established.

If in the mathematical model of the forward and inverse EIT problems the electrodes are modeled continuously, the boundary conditions of Eqs. (11) and (12) will exist simultaneously. In this case, the mapping that results in the continuous potential distribution $\sigma \left.\dfrac{\partial u}{\partial n}\right|_{\partial\Omega} = g$ for the continuous current distribution $u|_{\partial\Omega} = f$ is called the continuous current-to-voltage mapping, or the mapping of Neumann's conditions to Dirichlet's boundary conditions. The mapping of continuous surface induced voltage to the intensity distribution of injected continuous current on the object surface is the inverse of the Neumann-Dirichlet mapping. Λ_σ is the conventional symbol for voltage-current mapping or Dirichlet-Neumann mapping. This mapping is expressed as follows[17, 32]:

$$\Lambda_\sigma f = g \tag{19}$$

In this case, the current-voltage or Newman-Dirichlet mapping is defined as follows[17, 32]:

$$\Lambda_\sigma^{-1} g = f \tag{20}$$

By examining the boundary conditions in the continuous and complete model of the electrode, it can be seen that the current-voltage and voltage-current mapping operators are linear[17, 32].

2.3.1 Forward problem in EIT

In the forward problem, the distribution of electrical conductivity σ and one of the boundary conditions including peripheral voltage (Dirichlet condition) or peripheral current (Neumann condition) are known; The purpose of solving Eq. (9) with one of the boundary conditions of Eq. (10) is to find the complementary boundary condition.

Definition 3 In the complete model of electrodes, the direct Dirichlet problem is to find the Neumann boundary values of current intensity in current injecting electrodes I by having the σ distribution U and Dirichlet conditions[17, 32].

$$U \xrightarrow{R^{-1}} I \tag{21}$$

The operator R^{-1} is a discretized version of Dirichlet-Neumann mapping. In fact, this operator is the electrical conductivity matrix, which is obtained by calculating the electrical resistance matrix and calculating its inverse R.

Definition 4 In the complete model of electrodes, Neumann's direct problem is to find the Dirichlet boundary values U by having Neumann's distribution σ and conditions I[17, 32],

$$I \xrightarrow{R} U \tag{22}$$

2.3.2 Inverse problem in EIT

In the inverse problem of electrical impedance tomography, both parts of the current-voltage mapping are known as a pair of boundary data. The purpose of solving the inverse problem is to find the distribution of electrical conductivity σ inside the object Ω using these specific binaries.

Definition 5 In the complete electrode model, the

inverse problem is to find σ with the discrete voltage-current mapping R^{-1} or current-voltage mapping R[10],

$$R^{-1} \rightarrow \sigma \tag{23}$$

So far, various theorems about the existence of the answer and its uniqueness in the inverse problem have been presented. In these theorems, whose difference is in the functional space considered for the answer u, the goal is to show that Λ_σ can be obtained by having a complete mapping σ. But in practice, due to the situation of defining the inverse problem, it is difficult to find a unique and correct answer for the inverse problem by considering the complete model of the electrodes[32].

In connection with the inverse problem in two-dimensional space, Nachamn was the first to provide a proof for the uniqueness of the answer[33]. In his approach, special conditions of smoothness for σ and the boundary of the object are considered. The feature of Nachman's proof is that it provides a constructive way to solve the inverse problem and obtain the image σ. Based on his proof, a Finnish researcher, Siltanen, presented an algorithm called D-bar, which is able to solve the inverse nonlinear problem without repeating and optimizing electrical conductivity values and obtained an image of σ[34]. The distribution smoothness condition σ in D-bar algorithm has been reduced by other researchers, such as Brown et al.[35] and Astala et al.[36] In the next part of the article, the electrodes and their different arrangement models around the target object are introduced and the complete model of the electrode is examined in detail.

3 Electrode

An electrode is a type of converter that converts the electric current of a wire into an ion current in an electrolyte. In reconstructing the impedance images, the value of the contact impedance between the electrode and the object should be low and clear. Electrodes are made of materials， such as gold, platinum, and silver chloride[3, 5, 15, 22]. In the modeling of the electrodes, the impedance of the contact point of the electrodes with the surface of the object should be considered. The larger the electrode dimensions, the smaller the contact impedance[3].

By increasing the dimensions of the electrode, the reading error of the electrode voltage also decreases. The physical position of the electrodes and their image in the model has a great impact on the accuracy of the reconstructed image[8, 17, 25, 30, 37]. Therefore, four different types of models for electrodes can be considered in solving the EIT inverse problem.

3.1 Electrode patterns

3.1.1 Adjacent pattern

This method, also known as the neighborhood method, is the most famous impedance measurement method. As shown in Fig. 2, the current is injected into the object through two adjacent electrodes, and the voltage on the rest of the electrodes is measured two by two. Then the current is injected through the next two adjacent electrodes and the voltage values are measured in the same way. This procedure is repeated on each pair of adjacent electrodes[3].

In this convention, the current has less penetration in the internal layers of the object's impedance. Therefore, this measurement pattern is sensitive to impedance changes near the electrodes, and is less sensitive to impedance changes at far points[3].

3.1.2 Opposite pattern

In this model, every time the pair of electrodes that are right opposite each other (and make an angle of 180°) inject the current, the resulting voltage is measured on the rest of the electrodes around the object. The most common method of voltage measurement is to consider one of the electrodes that is exactly adjacent to the injection electrodes as the reference electrode. Figure 3 shows this pattern. In this method, more details of the impedance of the internal points of the object are obtained[8].

3.1.3 Cross pattern

In this model, two adjacent electrodes are used as current and voltage reference. As shown in Fig. 4, first the current is injected through electrodes 16 and 2, and 13 voltage differences between electrode 1 and other electrodes are measured. Then, the current is injected

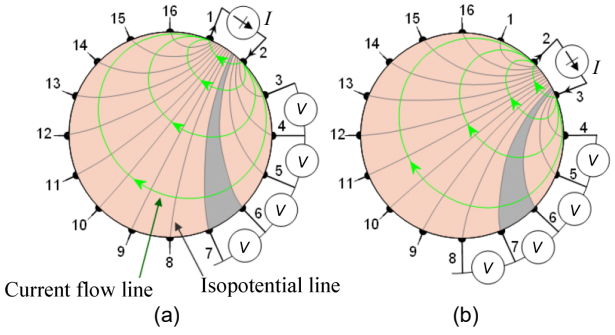

Fig. 2 Adjacent pattern in EIT, (a) current injection and (b) voltage measurement[8].

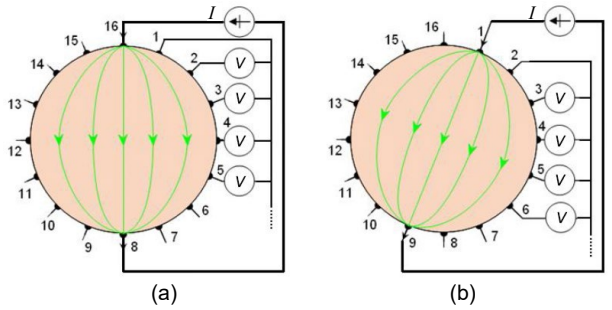

Fig. 3 Opposite pattern in EIT, (a) current injection and (b) voltage measurement[8].

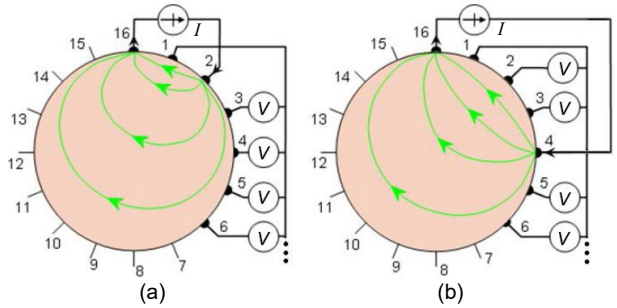

Fig. 4 Cross pattern in EIT, (a) current injection and (b) voltage measurement[8].

through electrodes 16 and 4, and the voltage between electrode number 1 and other electrodes is measured. Using this model, 91 voltage values are measured on a 16-electrode system. This pattern is more sensitive to the impedance in the internal points of the object[8].

In the next part of the article, the electrical properties of concrete are examined, and some factors affecting the electrical conductivity of concrete are introduced. Also, the electric circuit equivalent to the crack, and its relationships are presented.

4 Electrical Properties of Concrete

4.1 Concrete cracks factors

The creation of cracks in cement structures, such as those made of reinforced concrete, may be caused by various factors, including forces that enter the structure from outside, volume loss of concrete, poor construction methods, and many other factors[38].

Repairing damaged concrete structures is often more economical than building new structures, especially if the damage to the structure happens in a short period of time after its construction. For this purpose, concrete structures, such as bridge decks, concrete slabs, dams, and tunnels need periodic inspection using Non-Destructive Testing (NDT) methods to check the entire structure[38].

The presence of cracks or cracks in concrete is a sign of damage and defect. These cracks can have different causes:

- mechanical (restrictions that are not foreseen);
- physical (temperature changes, etc.);
- chemicals (reaction of concrete with inducers or as a result of concrete shrinkage in the environment).

It should be noted that the technical impossibility of breaking the concrete sample confirms that these cracks and damages are studied and investigated only in the desired location[38, 39].

Several methods have been proposed for the automatic evaluation of the structural health of concrete structures. In general, many of these methods require the deployment of external sensors to measure the general and local structural responses to loading.

The best method for automatic evaluation of structural health of concrete structures is to use existing sensors in the field of non-destructive evaluation[40].

Currently, non-destructive testing methods are used in the construction industry to answer such issues. Several different methods are used to investigate and study cracks and delamination of concrete. Among these methods, impact method[41], ultrasonic pulse echo method[42], acoustic effect (sound) method[43], ground penetrating radar method[44], and infrared tomography (thermography) method are often used[38, 39, 45].

Electrical methods are different in terms of cost and ease of use, and are suitable for examining large concrete structures[38].

4.2 Electrical conductivity in materials containing cement

Conductivity (σ) is a main characteristic of materials. Materials containing cement, which have a conductivity coefficient from 10^{-3} to 10^{-6} S/cm, are introduced as semiconductors[46]. Since the ions in water are the primary charge carriers, the conductivity of materials containing cement naturally has a strong dependence on the amount of moisture[46].

In recent years, considerable attention has been paid to the measurement and interpretation of the electrical properties of cement composites, including reinforced concrete. In particular, the electrical properties of cement can be used to evaluate the microstructural details of the material[47]. In the following, the electrical equivalent circuit of the concrete crack is introduced.

4.3 Equivalent electrical model of crack and impurities

The crack model is supposed to contain a specific density of concrete structures. The schematic of the electrical equivalent circuit of the crack is made of N_r electrical resistors that are connected in parallel. Figure 5 shows the equivalent electrical circuit of the crack. The value of electrical resistance in each block of the crack reveals the composition of its ingredients, including air, water, dust, or cement. Two parameters of crack depth (far or near from the surface) and crack size (specific weight) affect the crack equivalent strength[38],

$$\frac{1}{R_{\text{eq}}} = \sum_{i=1}^{n}\left(\alpha_i \frac{1}{R_i}\right) \tag{24}$$

$$\sum_{i=1}^{n} \alpha_i = 1 \tag{25}$$

The equivalent resistance (R_{eq}) is derived from the average of the local resistances (R_i). A distance factor from the surface (α_i) is applied to each of the local resistances[38]. The greater the depth of the crack, the greater the distance factor from the surface. The sum of the factors of the distance from the surface during the crack is equal to one[38].

5 EIT System Hardware

The process of collecting data and reconstructing the image is carried out by injecting a precise alternating electric current to the peripheral boundaries of the object, measuring the voltage in the peripheral boundaries, transferring the data to the computer, and processing the collected data with software. Matlab and special reconstruction algorithms are used. As seen in Fig. 6, the top view of the electrical impedance tomography system is described[48, 49].

The accuracy of the system hardware plays a very important and vital role in the quality of the final image. Figure 6 shows the main parts of the electrical impedance tomography system. The current source includes a Voltage Controlled Oscillator (VCO) as a waveform generator and a Voltage-to-Current Converter (VCC). The stability and accuracy of the injected current to the peripheral boundaries of the target object is done by this part with the help of multiplexers. Another task of this part is to generate pulses. These pulses are used to measure the peripheral voltage of the voltage demodulator blocks, and measure the voltage[48, 49].

6 Tests and Results of Image Reconstruction

In this section, the final images are reconstructed as

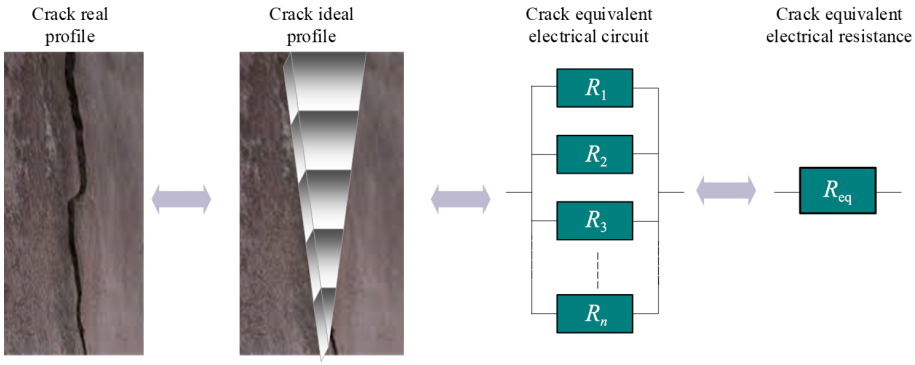

Fig. 5 Reconstruction of a crack for measurement of its electrical resistance[38].

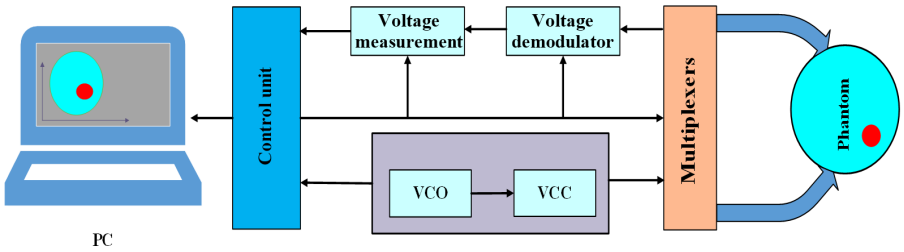

Fig. 6 Main block diagram of electrical impedance tomography system[48].

results using the EIT system. The block diagram of the EIT system is shown in Fig. 7. In this instrument, an ATMEGA128 microcontroller is used as the processing core of the control unit of the system. The control unit controls and form the current injection and voltage measurement patterns on the electrodes, and at the same time, measures the induced voltages by multiplexing Analog-to-Digital Converter (ADCs). The digital value of the measured voltage patterns is then communicated among the control unit and a PC. Table 1 summarizes the specification of the chief ingredient of the designed instrument. These tests are performed on cement samples without cracks containing a heterogeneous object in order to identify the position and type of the heterogeneous object inside the cement.

The experiments are performed using a 16-electrode phantom. The phantom used is a hollow cylinder made of Plexiglas with a height of 20 cm and a diameter of 20 cm, as shown in Fig. 8. Copper electrodes are located with equal distances around the phantom, and in complete connection with the material inside the phantom, and through them electric current is injected and electric voltage is measured.

Metal and plastic cylinders with a diameter of 5 cm and a height of 20 cm are placed inside the phantom in order to create different electrical impedance compared to the homogeneous surface.

The number of electrodes on the reconstructed image in all cases is such that the upper point of the reconstructed image shows the position of electrode number one, and the rest of the electrodes are placed clockwise to electrode 16.

In all the experiments of the proposed EIT system, the proximity model has been used to excite and measure the peripheral voltages.

6.1 16-electrode phantom experiments

6.1.1 Homogeneous medium

In this experiment, a 16-electrode phantom filled with concrete is used. As seen in Fig. 9, the EIT system sends 208 different voltages to the Matlab software after completing the imaging. Figure 9b shows the curve of the measured voltages. The voltages are higher near the injection electrodes and the curve has a peak at these points. Figure 9c shows the final reconstructed image of the phantom. According to the

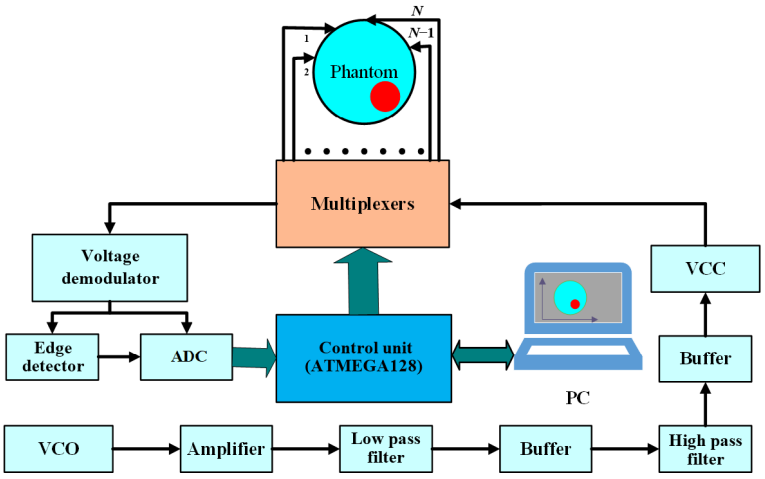

Fig. 7 Proposed assembled EIT system.

Table 1 Technical specifications of modules.

Ingredient	Technical Specification
Control unit	ATMEGA128
VCO	XR2206
Amplifier	AD844
Low-pass filter	LF412
ADC	AD1674
Analog multiplexer	ADG506AKN
Serial interface	MAX232

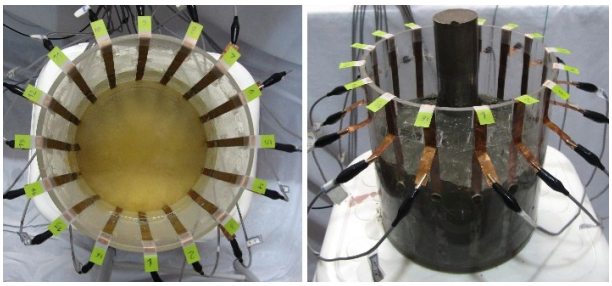

Fig. 8 16-electrode phantom made of plexiglass.

impedance bar next to the image, the impedance value of each point of the phantom can be recognized. The reconstructed image shows that there is no heterogeneous object in this phantom.

6.1.2 Heterogeneous medium with a metal rod in the vicinity of electrodes 2 and 3

As shown in Fig. 10, imaging that the 16-electrode phantom filled with concrete and a metal cylinder with a diameter of 5 cm is performed near the electrodes 2 and 3. Figure 10a shows the 16-electrode phantom containing concrete and a metal cylinder near electrodes 2 and 3. Figure 10b shows the measured voltage curve. The voltages near the injecting electrodes have a higher value, and the curve has a peak at these points. However, the voltage values near electrodes 2 and 3 have lower values due to the presence of the metal cylinder because, constant current creates a lower voltage value when passing through a low impedance. Therefore, the curve has a drop in these points. Figure 10c shows the final reconstructed image of the phantom. The final image includes a red mass near electrodes 2 and 3, which indicates an object with low electrical impedance (high electrical conductivity) near the electrode of interest. According to the impedance color bar next to the image, the impedance value of the mass in red can be recognized, which is the location of the metal cylinder.

6.1.3 Heterogeneous medium with a metal rod in the center

In this experiment, the aim is to image a 16-electrode phantom filled with concrete and a metal cylinder with a diameter of 5 cm in the center. Figure 11a shows the 16-electrode phantom containing concrete and a metal cylinder in its center. Figure 11b shows the measured voltage curve. The voltage values near the injecting electrodes are higher, and the curve has a peak at these points. Figure 11c shows the final reconstructed image of the phantom. The final image includes a mass in red in the center of the phantom, which indicates an object with low electrical impedance (high electrical conductivity) in the center of the phantom.

6.1.4 Heterogeneous medium with a plastic rod in the vicinity of electrodes 1 and 2

The purpose of this experiment is to image a 16-electrode phantom filled with concrete and a plastic cylinder with a diameter of 5 cm near electrodes 1 and 2.

Figure 12a shows the 16-electrode phantom containing concrete and a plastic cylinder near electrodes 1 and 2. Figure 12b shows the measured voltage curve. The voltage values near the injecting electrodes are higher, and the curve has a peak at these points. However, the voltage values near electrodes 1 and 2 have higher values due to the presence of the plastic cylinder because constant current creates a

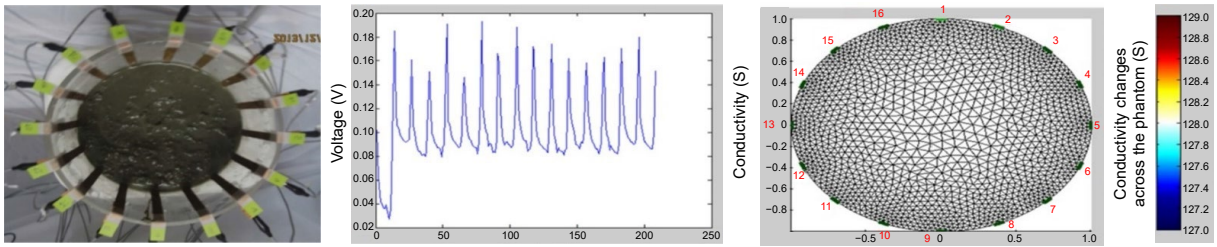

Fig. 9 16-electrode phantom in homogeneous medium and reconstruction of its images.

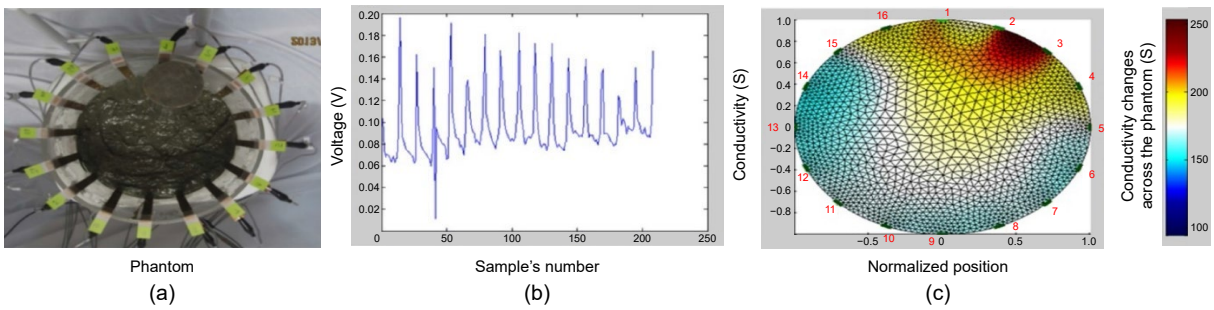

Fig. 10 16-electrode phantom in heterogeneous medium with metal rod adjacent to electrodes 2 and 3.

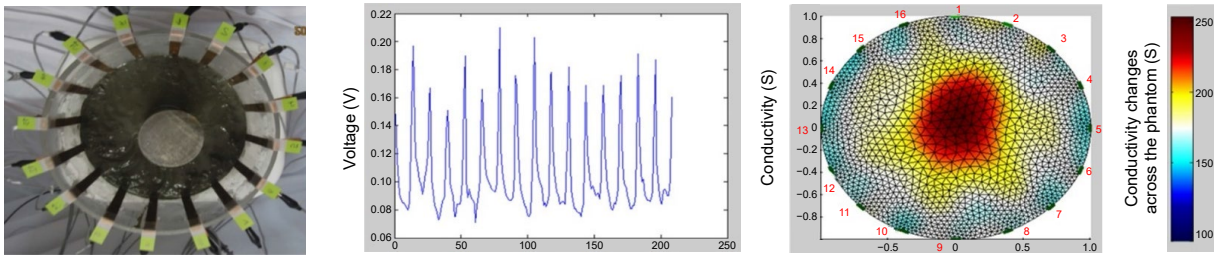

Fig. 11 16-electrode phantom in heterogeneous medium with metal rod in the center.

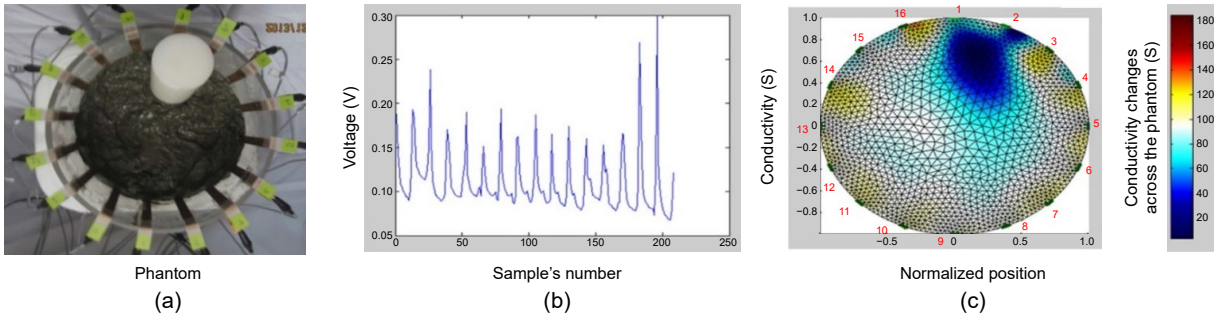

Fig. 12 16-electrode phantom in heterogeneous medium with plastic rod adjacent to electrodes 1 and 2.

higher voltage value when passing through a high impedance. Therefore, the curve has a peak at these points. Figure 12c shows the final reconstructed image of the phantom. The final image includes a mass in blue near electrodes 1 and 2, and indicates an object with high electrical impedance (low electrical conductivity) near electrodes 1 and 2.

6.1.5 Heterogeneous medium with a plastic rod in the center

The purpose of this experiment is to image a 16-electrode phantom filled with concrete and a plastic cylinder with a diameter of 5 cm in the center of the phantom. Figure 13a shows the 16-electrode phantom containing concrete and a plastic cylinder in its center. Figure 13b shows the measured voltage curve. The voltage values near the injecting electrodes are higher, and the curve has a peak at these points. Figure 13c shows the final reconstructed image of the phantom. The final image contains a mass in blue in the center of the phantom, and indicates an object with high electrical impedance (low electrical conductivity) in the center of the phantom.

7 Conclusion

In this paper, the design of a cheap and efficient impedance imaging system is introduced. By using the EIT imaging method, it is possible to reconstruct images of the internal parts of objects, such as concrete or human body. In the proposed design, an algorithm for reconstruction of the cross-sectional image of a conductive body, as well as different patterns of excitation and voltage measurement, are investigated.

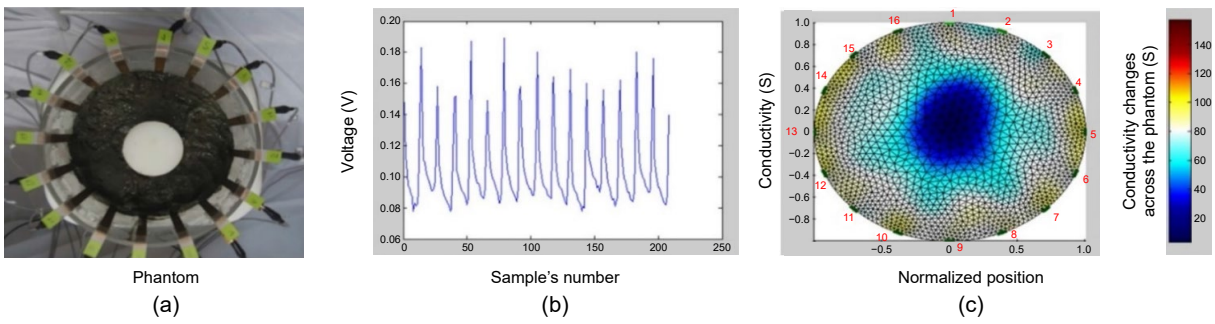

Fig. 13 16-electrode phantom in heterogeneous medium with plastic rod in center.

In addition to the imaging instrument, an imaging phantom is designed and prototyped. Inside this phantom, different homogeneous/inhomogeneous materials would be experimented by EIT system. For this purpose, the equivalent electrical impedance model of the concrete and its impurities inside a phantom are studied.

To analyze the accuracy and efficiency of the instrumented device, five different imaging experiments are performed on the 16-electrode phantom with different mixtures of concrete and impurities of plastic or metal. In each experiment, the accurate position and impedance of the metal or plastic cylinders inside the phantom are discovered. The results show that the EIT system has a high accuracy in detecting the location and type of impurity in concrete.

References

[1] L. Kong, G. Li, W. Rafique, S. Shen, Q. He, M. R. Khosravi, R. Wang, and L. Qi, Time-Aware missing healthcare data prediction based on ARIMA model, *IEEE/ACM Trans. Comput. Biol. Bioinform.*, doi: 10.1109/TCBB.2022.3205064.

[2] X. Zhou, X. Yang, J. Ma, and K. I. K. Wang, Energy-efficient smart routing based on link correlation mining for wireless edge computing in IoT, *IEEE Internet Things J.*, vol. 9, no. 16, pp. 14988–14997, 2022.

[3] X. Zhou, W. Liang, K. Yan, W. Li, K. I. K. Wang, J. Ma, and Q. Jin, Edge-enabled two-stage scheduling based on deep reinforcement learning for internet of everything, *IEEE Internet Things J.*, vol. 10, no. 4, pp. 3295–3304, 2023.

[4] C. R. Bull, R. Zwiggelaar, and R. D. Speller, Review of inspection techniques based on the elastic and inelastic scattering of X-rays and their potential in the food and agricultural industry, *J. Food Eng.*, vol. 33, nos. 1&2, pp. 167–179, 1997.

[5] Y. Liu, J. Cheng, L. Zhang, Y. Xing, Z. Chen, and P. Zheng, A low-cost dual energy CT system with sparse data, *Tsinghua Science and Technology*, vol. 19, no. 2, pp. 184–194, 2014.

[6] F. M. Bengel, T. Higuchi, M. S. Javadi, and R. Lautamäki, Cardiac positron emission tomography, *J. Am. Coll. Cardiol.*, vol. 54, no. 1, pp. 1–15, 2009.

[7] J. Liu, M. Li, J. Wang, F. Wu, T. Liu, and Y. Pan, A survey of MRI-based brain tumor segmentation methods, *Tsinghua Science and Technology*, vol. 19, no. 6, pp. 578–595, 2014.

[8] G. Wang, Holder David S: Electrical impedance tomography, *BioMed. Eng. OnLine*, vol. 4, no. 1, p. 27, 2005.

[9] C. Li, N. Duric, P. Littrup, and L. Huang, In vivo breast sound-speed imaging with ultrasound tomography, *Ultrasound Med. Biol.*, vol. 35, no. 10, pp. 1615–1628, 2009.

[10] J. P. Kruth, M. Bartscher, S. Carmignato, R. Schmitt, L. De Chiffre, and A. Weckenmann, Computed tomography for dimensional metrology, *CIRP Annals*, vol. 60, no. 2, pp. 821–842, 2011.

[11] L. Kong, L. Wang, W. Gong, C. Yan, Y. Duan, and L. Qi, LSH-aware multitype health data prediction with privacy preservation in edge environment, *World Wide Web*, vol. 25, no. 5, pp. 1793–1808, 2022.

[12] L. Qi, W. Lin, X. Zhang, W. Dou, X. Xu, and J. Chen, A correlation graph based approach for personalized and compatible web APIs recommendation in mobile APP development, *IEEE Trans. Knowl. Data Eng.*, vol. 35, no. 6, pp. 5444–5457, 2023.

[13] X. Fan, M. Dai, C. Liu, F. Wu, X. Yan, Y. Feng, Y. Feng and B. Su, Effect of image noise on the classification of skin lesions using deep convolutional neural networks, *Tsinghua Science and Technology*, vol. 25, no. 3, pp. 425–434, 2020.

[14] X. Zhou, Y. Hu, J. Wu, W. Liang, J. Ma, and Q. Jin, Distribution bias aware collaborative generative adversarial network for imbalanced deep learning in industrial IoT, *IEEE Trans. Ind. Inform.*, vol. 19, no. 1, pp. 570–580, 2023.

[15] X. Zhou, X. Xu, W. Liang, Z. Zeng, and Z. Yan, Deep-learning-enhanced multitarget detection for end-edge-cloud surveillance in smart IoT, *IEEE Internet Things J.*, vol. 8, no. 16, pp. 12588–12596, 2021.

[16] L. Qi, Y. Yang, X. Zhou, W. Rafique, and J. Ma, Fast anomaly identification based on multiaspect data streams for intelligent intrusion detection toward secure industry 4.0, *IEEE Trans. Ind. Inform.*, vol. 18, no. 9, pp. 6503–6511, 2022.

[17] H. Attar, H.Issa, J. Ababneh, M. Abbasi, A. Solyman, M. R. Khosravi, and R. S. Agieb, 5G system overview for ongoing smart applications: Structure, requirements, and specifications, *Computational Intelligence and Neuroscience*, doi: 10.1155/2022/2476841.

[18] B. Hobbs and M. T. Kebir, Non-destructive testing techniques for the forensic engineering investigation of reinforced concrete buildings, *Forensic Sci. Int.*, vol. 167, nos. 2&3, pp. 167–172, 2007.

[19] M. Kumar, P. Mukherjee, S. Verma, N. Kavita, J. Shafi, M. Wozniak, and M. F. Ijaz, A smart privacy preserving framework for industrial IoT using hybrid meta-heuristic algorithm, *Sci. Rep.*, vol. 13, no. 1, p. 5372, 2023.

[20] F. Wang, H. Zhu, G. Srivastava, S. Li, M. R. Khosravi, and L. Qi, Robust collaborative filtering recommendation with user-item-trust records, *IEEE Trans. Comput. Soc. Syst.*, vol. 9, no. 4, pp. 986–996, 2022.

[21] B. H. Brown, D. C. Barber, and A. D. Seagar, Applied potential tomography: Possible clinical applications, *Clin. Phys. Physiol. Meas.*, vol. 6, no. 2, pp. 109–121, 1985.

[22] B. H. Brown and A. D. Seagar, The Sheffield data collection system, *Clin. Phys. Physiol. Meas.*, vol. 8, pp. 91–97, 1987.

[23] T. I. Oh, E. J. Woo, and D. Holder, Multi-frequency EIT system with radially symmetric architecture: KHU Mark1, *Physiol. Meas.*, vol. 28, no. 7, pp. S183–S196, 2007.

[24] M. Cheney, D. Isaacson, and J. C. Newell, Electrical impedance tomography, *SIAM Rev.*, vol. 41, no. 1, pp. 85–101, 1999.

[25] D. Isaacson and M. Cheny, Effects of measurement precision and finite numbers of electrodes on linear impedance imaging algorithms, *SIAM J. Appl. Math.*, vol. 51, no. 6, pp. 1705–1731, 1991.

[26] R. A. Willoughby, Solutions of ill-posed problems (AN Tikhonov and VY Arsenin), *SIAM Review*, vol. 21, p. 266, 1979.

[27] A. Giannakidis and M. Petrou, Conductivity imaging and generalized radon transform: A review, in *Advances in Imaging and Electron Physics*, P. W. Hawkes, ed. Pittsburgh, PA, USA: Academic Press, 2010, pp. 129–172.

[28] F. Wang, L. Wang, G. Li, Y. Wang, C. Lv, and L. Qi, Edge-cloud-enabled matrix factorization for diversified APIs recommendation in mashup creation, *World Wide Web*, vol. 25, no. 5, pp. 1809–1829, 2022.

[29] E. Somersalo, M. Cheney, and D. Isaacson, Existence and uniqueness for electrode models for electric current computed tomography, *SIAM J. Appl. Math.*, vol. 52, no. 4, pp. 1023–1040, 1992.

[30] D. Isaacson, Distinguishability of conductivities by electric current computed tomography, *IEEE Trans. Med. Imaging*, vol. 5, no. 2, pp. 91–95, 1986.

[31] K. S. Cheng, D. Isaacson, J. C. Newell, and D. G. Gisser, Electrode models for electric current computed tomography, *IEEE Trans. Biomed. Eng.*, vol. 36, no. 9, pp. 918–924, 1989.

[32] L. Borcea, Electrical impedance tomography, *Inverse Problems*, vol. 18, no. 6, pp. R99–R136, 2002.

[33] A. I. Nachman, Global uniqueness for a two-dimensional inverse boundary value problem, *Ann. Math.*, vol. 143, no. 1, pp. 71–96, 1996.

[34] S. Siltanen, J. Mueller, and D. Isaacson, An implementation of the reconstruction algorithm of A Nachman for the 2D inverse conductivity problem, *Inverse Problems*, vol. 16, no. 3, pp. 681–699, 2000.

[35] R. M. Brown and G. A. Uhlmann, Uniqueness in the inverse conductivity problem for nonsmooth conductivities in two dimensions, *Communications in Partial Differential Equations*, vol. 22, nos. 5&6, pp. 1009–1027, 1997.

[36] K. Astala, J. L. Mueller, L. Päivärinta, and S. Siltanen, Numerical computation of complex geometrical optics solutions to the conductivity equation, *Appl. Comput. Harmon. Anal.*, vol. 29, no. 1, pp. 2–17, 2010.

[37] J. F. P. J. Abascal, S. R. Arridge, D. Atkinson, R. Horesh, L. Fabrizi, M. De Lucia, L. Horesh, R. H. Bayford, and D. S. Holder, Use of anisotropic modelling in electrical impedance tomography; description of method and preliminary assessment of utility in imaging brain function in the adult human head, *NeuroImage*, vol. 43, no. 2, pp. 258–268, 2008.

[38] J. F. Lataste, C. Sirieix, D. Breysse, and M. Frappa, Electrical resistivity measurement applied to cracking assessment on reinforced concrete structures in civil engineering, *NDT E Int.*, vol. 36, no. 6, pp. 383–394, 2003.

[39] K. Karhunen, A. Seppänen, A. Lehikoinen, P. J. M. Monteiro, and J. P. Kaipio, Electrical resistance tomography imaging of concrete, *Cem. Concr. Res.*, vol. 40, no. 1, pp. 137–145, 2010.

[40] S. K. Dwivedi, M. Vishwakarma, and A. Soni, Advances and researches on non destructive testing: A review, *Mater. Today*: *Proc.*, vol. 5, no. 2, pp. 3690–3698, 2018.

[41] H. Wiggenhauser, C. Köpp, J. Timofeev, and H. Azari, Controlled creating of cracks in concrete for non-destructive testing, *J. Nondestruct. Eval.*, vol. 37, no. 3, p. 67, 2018.

[42] A. Ndagi, A. A. Umar, F. Hejazi, and M. S. Jaafar, Non-destructive assessment of concrete deterioration by ultrasonic pulse velocity: A review, *IOP Conf. Ser.*: *Earth Environ. Sci.*, vol. 357, p. 012015, 2019.

[43] B. F. Ji and W. L. Qu, The research of acoustic emission techniques for non destructive testing and health monitoring on civil engineering structures, in *Proc. Int. Conf. Condition Monitoring and Diagnosis*, Beijing, China, 2008, pp. 782–785.

[44] S. Li, X. Gu, X. Xu, D. Xu, T. Zhang, Z. Liu, and Q. Dong, Detection of concealed cracks from ground penetrating radar images based on deep learning algorithm, *Constr. Build. Mater.*, vol. 273, p. 121949, 2021.

[45] A. Mohan and S. Poobal, Crack detection using image processing: A critical review and analysis, *Alex. Eng. J.*, vol. 57, no. 2, pp. 787–798, 2018.

[46] T. C. Hou and J. P. Lynch, Electrical impedance tomographic methods for sensing strain fields and crack damage in cementitious structures, *J. Intell. Mater. Syst. Struct.*, vol. 20, no. 11, pp. 1363–1379, 2009.

[47] G. Trtnik and M. Gams, Recent advances of ultrasonic testing of cement based materials at early ages, *Ultrasonics*, vol. 54, pp. 66−75, 2014.

[48] M. Khalighi, B. V. Vahdat, M. Mortazavi, W. Hy, and M. Soleimani, Practical design of low-cost instrumentation for industrial electrical impedance tomography (EIT), in *Proc. IEEE Int. Instrumentation and Measurement Technology Conf. Proc.*, Graz, Austria, 2012, pp. 1259–1263.

[49] L. Horesh, Some novel approaches in modelling and image reconstruction for multi-frequency electrical impedance tomography of the human brain, PhD dissertation, University College London, London, UK, 2006.

Abolfazl Roshanpanah received the BEng and MEng degrees in electrical engineering from Islamic Azad University, Iran in 2011 and 2013, respectively. Since 2016, he has been working toward the PhD degree in electrical engineering at Islamic Azad University, Science and Research Branch, Tehran, Iran. His research interests include the design of current-mode high-speed data converters for data communication systems, electrical imaging tomography, and digital systems.

Hani Attar received the PhD degree from University of Strathclyde, UK in 2011. Since 2011, he has been working as a researcher of electrical engineering and energy systems. He is now a lecturer at Zarqa University, Jordan. His research interests include renewable energy systems, efficient computing & design, cyber-physical systems, and wireless communications.

Mohammad R. Khosravi received the BEng degree in electrical engineering from Shiraz University, Iran in 2013, and the MEng degree in electrical engineering from Persian Gulf University, Iran in 2015. He completed his academic research to earn the PhD degree in communications engineering from Shiraz University of Technology, Iran from 2016 to 2020. Later on, he joined the industry sector to develop some related industrial research from 2020 to 2022 as a part of his scientific commitments. Currently he is working at Department of Computer Engineering, Persian Gulf University, Iran. His main topics of interest are multimedia systems, as well as high-performance computing and communications.

Mahdi Abbasi received the BEng and MEng degrees in computer engineering from Sharif University of Technology, Tehran, Iran, and the PhD degree in computer engineering from University of Isfahan, Isfahan, Iran. He is currently an associate professor at Department of Computer Engineering, Bu-Ali Sina University, Hamedan, Iran. His research interests include innovative computer architecture, network optimization, and digital systems.

Ayman Amer received the PhD degree from Tennessee University, USA in 1991. He is the dean of the Department of Energy Engineering, Zarqa University, Jordan, and his research interest topics are renewable energy efficiency and energy storage. Moreover, smart design for energy efficiency is regarded as an interesting topic for his research.

Ahmed A. Solyman received the BEng and MEng degrees in electrical and electronics engineering from Military Technical College, Egypt in 1999 and 2006, respectively, and the PhD degree in electrical and electronics engineering from University of Strathclyde, UK in 2013. He is currently an assistant professor at Department of Electrical and Electronics Engineering, Faculty of Engineering and Architecture, Nişantaşı University, Turkey. His research interests include wireless communication networks, IoT, smart grid, artificial intelligence, and renewable energy systems.